

# Potential of CO<sub>2</sub> capture from flue gases by physicochemical and biological methods: a comparative study

Ismael Matito-Martos<sup>a,¶</sup>, Claudia Sepúlveda<sup>b,¶\*</sup>, Cintia Gómez<sup>c</sup>, Gabriel Acién<sup>c\*</sup>, Julio Perez-Carbajo<sup>a</sup>, José A. Delgado<sup>d</sup>, V. I. Águeda<sup>d</sup>, Conchi Ania<sup>e</sup>, José B. Parra<sup>f</sup>, Sofía Calero<sup>a,g</sup> and Juan A. Anta<sup>a\*</sup>

¶ These authors contributed equally to this work.

<sup>a</sup>*Department of Physical, Chemical and Natural Systems, University Pablo de Olavide, Sevilla 41013, Spain*

<sup>b</sup>*Bio-innovation Centre, Antofagasta Institute, University of Antofagasta, Chile*

<sup>c</sup>*Department of Chemical Engineering, University of Almería, 04120 Almería, Spain*

<sup>d</sup>*Department of Chemical Engineering, Universidad Complutense de Madrid, 28040, Madrid, Spain*

<sup>e</sup>*CEMTHI (CNRS UPR 3079) Université d'Orléans, 45071, Orléans, France.*

<sup>f</sup>*Instituto Nacional del Carbón, INCAR, CSIC, P.O. 73, 33080 Oviedo, Spain.*

<sup>g</sup>*Materials Simulation and Modelling, Department of Applied Physics, Eindhoven University of Technology, 5600MB Eindhoven, The Netherlands*

Corresponding authors\*: Gabriel Acién (facien@ual.es), Juan A. anta ([anta@upo.es](mailto:anta@upo.es))

KEYWORDS: CO<sub>2</sub> capture, zeolites, microalgae, light efficiency

## Abstract

The industrial viability of two emerging technologies for CO<sub>2</sub> capture from flue gases, i.e., adsorption in porous commercial zeolites and biomass production by microalgae, is compared. Our study is organized in two steps: first, the best system is selected (either zeolite type or microalgae strain). Second, their performance is quantified and their advantages at real conditions discussed. For the physicochemical process, we find that commercial zeolite MFI is the best choice for CO<sub>2</sub> capture from a typical industrial flue gas emission. Numerical dual PSA cycle simulations at ambient conditions yield 8 kg m<sup>-3</sup> bed h<sup>-1</sup> and an energy consumption of 0.987 MJ per kg of captured CO<sub>2</sub>. As regards the biological process, evaluation of several microalgae strains in continuous mode using low cost resources (waste water, fertilizers, flue gases), results in *Scenedesmus almeriensis* as the most promising strain. The maximal capacity of CO<sub>2</sub> capture at laboratory conditions was 0.1 kg m<sup>-3</sup> h<sup>-1</sup>, allowing to produce up to 0.06 of kg m<sup>-3</sup> h<sup>-1</sup> of biomass (3% maximal photosynthetic efficiency). Although this is a significantly lower value, the produced biomass, being composed by carbohydrates, entails an overall economic yield of 0.6 € m<sup>-3</sup>·day. To demonstrate reliability at large scale, experiments were performed in a 100 m<sup>2</sup> pilot raceway reactor under outdoor conditions. We measured 54 g of CO<sub>2</sub>/m<sup>2</sup>·day (= 197 tn/ha·year) and a biomass productivity of 21 g/m<sup>2</sup>·day (= 75 tn/ha·year). The energy consumption approaches to 0.48 MJ/kgCO<sub>2</sub>, lower than zeolites adsorption. Still, zeolites can be advantageous as they offer higher productivity, lower energy consumption than amines-based methods, and possibility of producing added-value chemical products, such as methanol, CO or CH<sub>4</sub>.

## 1. INTRODUCTION

The relationship between Global Warming and increasing emissions of Green House Gases (GHG) is not more under discussion, as most of the countries have signed the Paris Protocol to mitigate the anthropogenic emissions of these gases.<sup>1</sup> Thus, countries are enforced to implement real mitigation strategies considering reduction of GHG emission both by improvement of the technology for energy production and the development of technologies for GHG capture. Among the different GHG, carbon dioxide is one of the most relevant for the larger magnitude of its emission, mainly related with energy production from fossil fuels.<sup>2</sup> A reduction in power consumption or improvements to combustion processes can help reducing CO<sub>2</sub> emissions. Alternatively, carbon capture and storage (CCS) shows great potential in diminishing the amount of CO<sub>2</sub> released into the atmosphere from industrial and civil combustion processes<sup>3,4</sup>. CCS refers to strategies for capturing CO<sub>2</sub> from flue gases followed by long-term storage for hundreds of years; these are capable of contributing up to 55 % to the mitigation effort<sup>3</sup>. Different technologies have been proposed for CO<sub>2</sub> capture,<sup>5</sup> the most conventional being based on amines-related absorption processes,<sup>6</sup> other using membranes<sup>7</sup> or including cryogenic processes<sup>8</sup> to capture the CO<sub>2</sub> from the flue gases. The major problems related with these technologies are the large energy consumption, the difficulty to recover the CO<sub>2</sub> gas, and its tolerance to the corrosive conditions imposed by the flue gases composition<sup>9</sup>. On the other hand, the utilization of porous materials for CO<sub>2</sub> adsorption in Pressure Switch Adsorption (PSA) processes has been also proposed.<sup>10</sup> This technology requires less energy and also facilitates the recovery of the CO<sub>2</sub> gas by using a readily available driving force such as the pressure difference between the high feed pressure for adsorption and a lower pressure for

desorption. However, PSA methods still rely on the availability of materials with improved properties in terms of CO<sub>2</sub> adsorption capacity and selectivity. Materials that have been thoroughly studied are mainly inorganic zeolites,<sup>11</sup> metal organic frameworks<sup>12</sup>, as well as the functionalization of these with room temperature ionic liquids<sup>13</sup> among others. It must be born in mind that whatever the CO<sub>2</sub> capture process is, energy consumption must remain low and, besides, the final product, in the form of a concentrated CO<sub>2</sub> stream, must be valorised.

As an alternative to chemical and physicochemical techniques, the utilization of microalgae for CO<sub>2</sub> capture process has also been proposed. This biological process has been reported to require less energy, thus it is potentially more sustainable from the environmental point of view. However, biological methods are also sensible to pollutants contained into the flue gases and their typical rate of CO<sub>2</sub> capture is lower than that of chemical processes.<sup>14,15</sup> In spite of that, they have the critical advantage of providing a final product (microalgae biomass) that would be more valuable than the CO<sub>2</sub> stream of the chemical and physicochemical methods, thus positively contributing to the economic sustainability of the entire process. There is a lot of studies about the application of microalgae for CO<sub>2</sub> capture, most of them related with the production of biofuels, all of them concluding that the reliability of the process is highly dependent on the strains tested, production scale/technology and final application of the biomass. Moreover, the large surface and the overall cost of the technology are actually bottlenecks for the commercial development of microalgae-based CO<sub>2</sub> capture processes.<sup>16-19</sup>

In the last years, the large scale production of microalgae is fast increasing mainly by two reasons: (i) the enlargement of the market as microalgae biomass is now included in

more food/feed products, and (ii) the improvement of the technology allowing to increase the biomass productivity, thus reducing the biomass production costs. Some important advances include the development of more robust strains (improved strains non genetically modified), improvement of energy utilization efficiency and mass transfer capacity on the reactors, and development of new downstream strategies and products.<sup>20-24</sup> These advances make the possibility of using microalgae for CO<sub>2</sub> capture process much more realistic today than twenty years ago, especially if combined with the treatment of other wastes as wastewater or manure.<sup>19,25</sup> Thus, the growth potential of microalgae-based methods can be up to 100 times faster than terrestrial plants, thus achieving productivities of 100 tn/ha·year in dry basis. To achieve these figures, large amounts of nutrients are required: for each tonne of biomass produced, it takes up to 2 tn CO<sub>2</sub>, 100 kg N and 10 kg P. This can actually be provided by flue gases and wastewater.<sup>20</sup> Additionally, large surfaces and adequate environmental conditions (light, temperature, etc..) are required, factors such as pH, temperature and light intensity have a great influence on the growth dynamics of microalgae as do the nutrients .<sup>26</sup>

The aim of this work is to re-think the CO<sub>2</sub> capture process taking into account the actual technology available in order to determine the real suitability of novel processes at different scales. We will focus our study on two emerging technologies: (1) zeolite-based CO<sub>2</sub> adsorption (physicochemical process) and (2) microalgae-based CO<sub>2</sub> capture (biological process). In both cases, a common composition of flue gas, with varying CO<sub>2</sub> concentrations, typical of industrial combustion activities, have been considered. On the one hand, a combination of molecular simulation, numerical modelling of the continuous PSA process and equilibrium adsorption experiments has been used to assess the

potentiality of CO<sub>2</sub> capture of the physicochemical method. On the other hand, a 100 m<sup>2</sup> pilot scale raceway reactor has been used to evaluate the capability of the biological process under real outdoor conditions in terms of biomass production and CO<sub>2</sub> capture efficiency. In both cases a previous screening has been done to select the optimum zeolite (physicochemical process) and the optimum microalgae strain (biological process). Figures from the reactor experiment allow to evaluate the energy consumption and cost of the biological process, and to compare it with their physicochemical counterpart. Considering final applications of the biomass the suitability of both processes at commercial scale is finally discussed.

## **2. MATERIALS AND METHODS**

### **2.1. Theoretical determination of adsorption isotherms in zeolites**

Adsorption isotherms were computed using Grand Canonical Monte Carlo (GCMC) simulations with the RASPA code.<sup>27,28</sup> Adsorbates and adsorbents were considered rigid and force fields and model extensively described and validated.<sup>29,30,31</sup> Details and parameters of the interaction model used for these molecules can be found in the Supporting Information (**Section A, Table S1**)

Six widely employed zeolites with different geometry and topology were selected for this work (i.e. BEA, FAU, FER, ITQ-29, MFI, and MOR). Most of them are commercially available and used for different gas separations. We use a pure-silica version of the zeolites, considering them as rigid frameworks as it is well-known that the effect of zeolite flexibility is usually small in adsorption studies.<sup>32</sup> A representation of the grid surface energy of the selected materials is presented in **Fig. S1**. A description of the morphology

and crystalline structure of these zeolites as considered in the modeling is also included in the Supporting Information (**Section B, Figure S2, Table S2**).

The insertion of molecules using Monte Carlo can take place in cavities or channels experimentally accessible only for some small adsorbates, such as H<sub>2</sub> or H<sub>2</sub>O. To avoid this artificial insertion of molecules and reproduce experimental behavior, these cavities need to be carefully blocked.<sup>33,34</sup> We use Monte Carlo to identify energetic preferential adsorption sites and Molecular Dynamics (MD) simulations to calculate the diffusion of the molecules. These sites from which molecules are unable to escape after 0.15 ns were properly blocked. In RASPA, the blockage is implemented using a list of geometric descriptions of the inaccessible volumes that are automatically considered as an overlap in MC simulations. Using this methodology, sodalites in FAU and ITQ-29 and y-axis channels in FER were blocked for all the molecules under study (except for H<sub>2</sub>O) due to narrow access windows do not allow diffusion of these molecules.

## **2.2 Experimental determination of adsorption isotherms in MFI zeolite**

Experimental equilibrium gas adsorption isotherms for pure gases (CO<sub>2</sub> and air) and for a mixture of 10 % CO<sub>2</sub> in air were recorded on pure silica MFI zeolite at room temperature using a volumetric analyser (Micromeritics) in the pressure range between 10<sup>-2</sup> and 120 kPa. The zeolite was outgassed under dynamic vacuum at 623 K (1K/min) overnight before the gas adsorption measurements. All the gases were supplied by Air Liquide with an ultra high purity (i.e., 99.995%). Pure silica MFI zeolite was supplied by Institute of Chemical Technology, CSIC, Spain

## 2.3 Pressure Swing Adsorption (PSA) simulations

Typical flue gas at ambient conditions mixture (0.75 N<sub>2</sub>, 0.10 CO<sub>2</sub>, 0.11 O<sub>2</sub>, and 0.032 H<sub>2</sub>O at 298 K and 1 bar) was considered in the PSA simulations. A simple Skartrom PSA cycle in *isothermal conditions* was first considered to compare the separation performance of the 6 zeolites used in **Section 2.1**, because the model resolution is faster than with more complex cycles. Although industrial PSA processes usually operate adiabatically, the isothermal conditions that can be achieved if the bed diameter are reduced and the heat exchange rate between the bed and the surroundings is increased. A detailed cycle description is presented in **Fig. S3** in the Supporting Information. Operating conditions and model parameters are given in **Table S3**. The high pressure ( $P_H$ ) of the cycle is defined to 1 bar to avoid the energy consumption on compressing the feed gas. A low pressure ( $P_L$ ) of 0.1 bar is used as it is a typical limit considered for practical application of PSA technology.<sup>35,36</sup> It is also assumed that the adsorbent crystals are agglomerated in pellets, and that mass transfer between gas and adsorbent is controlled by macropore diffusion, neglecting intracrystalline resistance.<sup>37</sup>

The multicomponent adsorption isotherms for the PSA simulations were obtained by applying the Ideal Adsorption Solution Theory (IAST)<sup>38</sup>, previously obtained by GCMC simulations. Isotherms were fitted with the Langmuir equation.<sup>39</sup> Details of the simulations and the fit are summarized in the Supporting Information (**Section C**)

To improve the yield of the CO<sub>2</sub> separation predicted in the previous PSA Skarstrom cycle, a dual-PSA cycle with three equalization steps in *adiabatic conditions*, with MFI zeolite as adsorbent in the bed was also implemented.<sup>40</sup> The dual-PSA cycle includes two coupled PSA cycles where one cycle increases the CO<sub>2</sub> concentration to an intermediate value



(rectifying PSA) and the other increases further the CO<sub>2</sub> concentration up to the desired specification (stripping PSA). The same PSA cycle has been used for each one of the coupled cycles. The individual PSA cycle is presented in **Fig. S4a** in the Supporting information. Light product and tail gas are obtained at 1 bar. The way of coupling the individual PSA cycles for the dual configuration is presented in **Fig. S4b**. Other parameters used in the simulations (except gas velocities) are given in **Table S3**. To model the effect of temperature on the adsorption isotherms, the pure adsorption isotherms of all the components in MFI have been obtained by GCMC simulation, and they have been fitted with the temperature dependent Langmuir model ( $q = K_{H0} \exp(-\Delta H/RT) p / (1 + b_0 \exp(-\Delta H/RT) p)$ ). A comparison between the fitted isotherms and the molecular simulation data is presented in **Fig. S6**, and the obtained Langmuir parameters are presented in **Table S6**.

## 2.4 Microorganisms and culture media

Different microorganisms, microalgae and cyanobacteria, were preselected according to previous experience and the literature; more than 40 reference works being reviewed in depth for that. Only robust strains suitable for large-scale production under non-optimally controlled conditions were selected (**Table S7** in the Supporting Information). Some of the microorganisms were already available at the University of Almeria whilst others were obtained from official culture collections, mainly from the Culture Collection of Algae and Protozoa (Oban, Scotland). Inoculum from all the strains were kept under controlled conditions in 1 L flasks, at 20 °C, under constant illumination at 200  $\mu\text{E}\cdot\text{m}^{-2}\cdot\text{s}^{-1}$  provided by fluorescent lamps, with constant aeration at 0.1 v/v/min with no CO<sub>2</sub> supply in a standard Arnon culture medium. The standard culture medium was prepared using freshwater and Mann & Myers medium prepared using fertilizers (0.14  $\text{g}\cdot\text{L}^{-1}$  K(PO<sub>4</sub>)<sub>2</sub>, 0.18  $\text{g}\cdot\text{L}^{-1}$

Mg(SO<sub>4</sub>)<sub>2</sub>, 0.9 g·L<sup>-1</sup> NaNO<sub>3</sub>, 0.02 mL·L<sup>-1</sup> Welgro, and 0.02 g·L<sup>-1</sup> Kalentol), it being autoclaved at 121 °C for 15 minutes only for laboratory trials. The inoculum cultures were monitored by microscopic observation using a Leica CME microscope 40X/0.65 to verify non-contamination.

## 2.5 Laboratory photobioreactors

Experiments were performed in bubble-column photobioreactors (~ 300 mL) aerated at 0.2 v/v/min with pH controlled at 8.0 by on-demand injection of real flue gas (from a diesel boiler). The temperature inside the reactors was kept at 25°C by controlling the temperature of the chamber in which the reactors are located. A total of 15 bubble-column reactors were used and each experiment was tested in triplicate. The reactors are illuminated artificially using fluorescent lamps that are automatically turned on or off to simulate the circadian solar cycle. Irradiance on the reactors surface ( $I_o$ ) varied throughout the day from zero to 1200  $\mu\text{E}\cdot\text{m}^{-2}\cdot\text{s}^{-1}$  at noon - using these values, a mean irradiance for the light period ( $I_{light}$ ) of 780  $\mu\text{E}\cdot\text{m}^{-2}\cdot\text{s}^{-1}$  was obtained. On a 24 h basis, the mean irradiance on the reactor surface ( $I_{day}$ ) was 390  $\mu\text{E}\cdot\text{m}^{-2}\cdot\text{s}^{-1}$ .

Experiments were performed in continuous mode. For this, we used inoculum from previous cultures developed in flasks but without pH control and under continuous illumination at 200  $\mu\text{E}\cdot\text{m}^{-2}\cdot\text{s}^{-1}$ . The volume of inoculum supplied to the reactors at the beginning of the experiment was 10% of the total culture volume in the bubble column. Once the reactor was inoculated, it was operated in batch mode for 5 days, after that it was operated in semicontinuous mode at 0.3 day<sup>-1</sup> dilution rate (medium inlet and harvesting are performed during illuminated period), till steady state was achieved (at least two times the

hydraulic retention time). During the experiments the cultures were daily monitored measuring the biomass concentration and the fluorescence of chlorophylls. Water evaporation was compensated for each day with distilled water to avoid changes in conductivity or of any nutrient in the culture broth. At the end of the experiment, when a steady state was achieved, the culture was harvested and the biomass was stored for biochemical composition analysis.

## **2.6 Outdoor raceway**

The raceway reactor is located at the “Las Palmerillas” Research Centre, 36° 48'N–2° 43'W, part of the Cajamar Foundation (Almería, Spain). The reactor consists of two 50 m long channels (0.46 m high × 1 m wide), both connected by 180° bends at each end, with a 0.59 m<sup>3</sup> sump (0.65 m long × 0.90 m wide × 1 m deep) located 1 m along one of the channels.<sup>41</sup> A paddlewheel system was used to recirculate the culture through the reactor at a regular velocity of 0.2 m·s<sup>-1</sup>, although it can be increased up to 0.8 m·s<sup>-1</sup> by manipulating the frequency inverter of the engine. The pH, temperature and dissolved oxygen in the culture were measured using appropriate probes (5083 T and 5120, Crison, Barcelona, Spain), connected to an MM44 control-transmitter unit (Crison Instruments, Spain), and data acquisition software (Labview, National Instruments) providing complete monitoring and control of the installation. The pH of the culture was controlled at 8.0 by on-demand injection of flue gas (from a diesel boiler), whereas temperature was not controlled; it ranged ±5°C with respect to the daily mean air temperature, which varied from 12°C in winter to 28°C in summer. The raceway reactor was inoculated and operated in batch mode for one week, after which it was operated in semi-continuous mode at 0.2 day<sup>-1</sup> at a culture

depth of 0.15 m. Only samples from steady-state conditions were used. Evaporation inside the reactor was compensated by the daily addition of fresh water.

## 2.7 Analytical methods

The cultures were examined daily under a microscope, an Olympus CH20 (Olympus Corp., USA), to evaluate the cell status and to detect possible contamination. Images of the cultures were photographed for further use. Absorbance and turbidity were measured daily to monitor the evolution of the cultures. The dry weight biomass concentration ( $C_b$ ) was measured by filtering 100 ml of culture through 1  $\mu\text{m}$  filters and drying it at 80°C in an oven over a 24 h period; this measurement was performed at the end of the culture. The dry weight biomass concentration values during the batch experiments were calculated from absorbance/turbidity measurements using the correlation obtained at the end of the batch culture. Biomass productivity was calculated as the product of the biomass concentration by the imposed dilution rate. The cell status was checked daily by measuring the chlorophyll fluorescence ( $F_v/F_m$ ) ratio with a fluorometer (AquaPen AP 100, Photon System Instruments, The Czech Republic). For this, the cells were adapted to the dark for 15 minutes prior to measurement. Absorbance in the visible range (400-700 nm) was measured daily using a double-beam Helios Alpha spectrophotometer and the extinction coefficient ( $K_a$ ) was calculated by dividing the average absorbance value by the biomass concentration ( $C_b$ ) and the cuvette's light path ( $d$ ):  $K_a = \text{Abs} / (C_b d)$ . The average irradiance inside the culture ( $I_{av}$ ) was calculated as a function of the irradiance at the surface ( $I_o$ ), the biomass extinction coefficient ( $K_a$ ), the biomass concentration ( $C_b$ ) and the light path inside the reactor ( $d$ ).<sup>42</sup>

$$I_{av} = \frac{I_{light}}{K_a C_b d} (1 - e^{-(K_a C_b d)}) \quad (1)$$

Because mean daily values were considered, irradiance during the light period ( $I_{light}$ ) was used as the irradiance on the reactor surface to calculate the mean daily irradiance. The Quantum yield ( $\Psi_E$ ) is defined as the amount of biomass ( $P_b$ ) generated by a unit of radiation (usually a mole of photons) absorbed by the culture. Since this represents the ratio of biomass generation to absorbed photon flux, it can be calculated using<sup>43</sup>

$$\Psi_E = \frac{P_b}{F_{vol}} \quad (2)$$

The photon flux absorbed through the reactor volume ( $F_{vol}$ ) is calculated from the average irradiance on a culture volume basis using<sup>43</sup>

$$F_{vol} = I_{av} \cdot K_a \cdot C_b \quad (3)$$

The photosynthetic efficiency (PE) is the fraction of energy fixed into biomass as a function of the combustion heat of the biomass that was considered constant ( $Q_b = 20 \text{ MJ/kg}$ )<sup>43</sup>

$$PE = \frac{P_b \cdot Q_b}{F_{vol}} \quad (4)$$

Freeze-dried biomass taken at the end of the batch culture was analysed. Lipids were determined gravimetrically from an extract obtained with chloroform:methanol (2:1) (v/v).<sup>44</sup> The protein content was determined using the modified Lowry method.<sup>45</sup> The moisture content was determined by weight losses after 24 h at 80 °C, whereas the ash

content was determined by calcination at 550 °C for 6 h. The carbohydrate content of the biomass was determined as the difference remaining from 100% after taking away the protein, lipid and ash content.

### 3. RESULTS

#### 3.1 CO<sub>2</sub> adsorption capacity of commercial zeolites: equilibrium properties and materials screening

The adsorption loadings in BEA, FAU, FER, ITQ-29, MFI, and MOR zeolites at near ambient conditions (298 K; and 1, 2 and, 10 bar) was obtained by GCMC simulation for three different typical flue gas mixtures (N<sub>2</sub> 75%; CO<sub>2</sub> 5%, 10%, and 15%; H<sub>2</sub>O at saturation conditions; and O<sub>2</sub> up to complete the mixture). **Fig. 1** shows the gas uptakes as a function of the total pressure of the system. We can observe that the inclusion of water is almost negligible in all structures, as could be expected due to the pure-silica nature of the used materials. Competition of water with the rest of adsorbates is unfavored by the hydrophobic character of material and also due the fact that is the smallest molecule under study (kinetic diameter of around 2.6 Å).<sup>46,47</sup> Oxygen, is also almost displaced from adsorption by the other molecules, whatever is the concentration of CO<sub>2</sub> in the mixture. Again, the size (i.e. kinetic diameter of 3.467 Å) and the low polarity of this molecule (quadrupole moment of ca. 0.39 D Å)<sup>46,47</sup> difficult its competition with the other gases. The overall performance strongly depends on the CO<sub>2</sub> fraction in the mixture, that is increased from 0.05 to 0.15 while the fraction of N<sub>2</sub> is fixed at 0.75. In the case of the lower concentration of CO<sub>2</sub>, N<sub>2</sub> prevails over CO<sub>2</sub> in almost all the zeolites. However, as soon as the CO<sub>2</sub> fraction is increased to 0.10, this molecule is able to displace N<sub>2</sub> from the main

adsorption sites of the frameworks. Both molecules have similar kinetic diameters and the higher quadrupole moment of CO<sub>2</sub> probably makes the difference between them (4.30 D Å and 1.52 D Å, for CO<sub>2</sub> and N<sub>2</sub> respectively). This effect is less visible in FAU, the structure with the highest pore volume, because there is almost no competition for the available space at our pressure conditions. This is supported by the low total loading in this structure, being in the range of the other two structures with the lowest pore volume and surface area (i.e. MOR and FER). Another interesting exception is the low reduction in N<sub>2</sub> uptake in MOR while increasing CO<sub>2</sub> mixture fraction. As we say, CO<sub>2</sub> displaces N<sub>2</sub> from the main adsorption sites, but this is not the case of the additional adsorption sites in MOR, where CO<sub>2</sub> is proved to not commensurate well.<sup>48</sup> CO<sub>2</sub> and N<sub>2</sub> Average Occupation Profiles (AOPs) for the three different gas mixture compositions at the highest pressure in MOR zeolite (**Fig. S7**) reveal that while CO<sub>2</sub> is always adsorbed in the main channels, N<sub>2</sub> migrates from the main channels to the side pockets in which it almost does not compete with CO<sub>2</sub>.

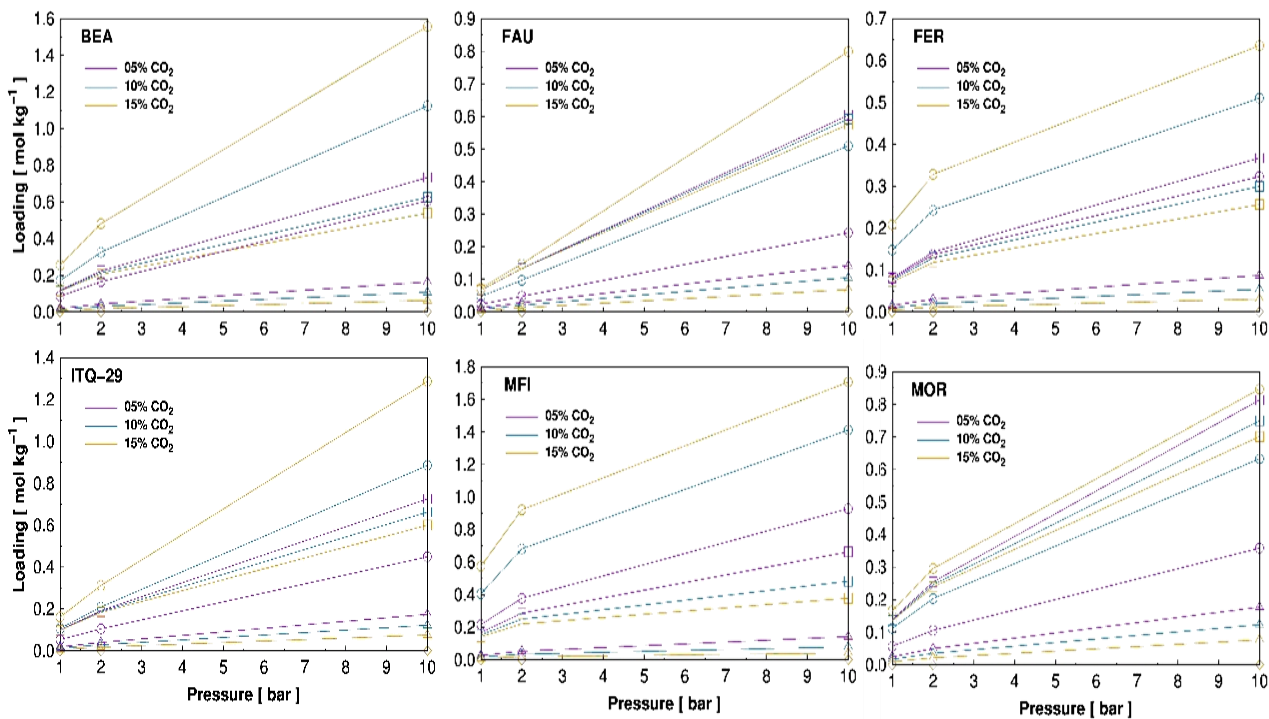


**Figure 1.** Adsorption loading of N<sub>2</sub> (squares), CO<sub>2</sub> (circles), O<sub>2</sub> (triangles), and H<sub>2</sub>O (diamonds) in BEA, FAU, FER, ITQ-29, MFI, and MOR zeolites at room temperature and 1, 2, and 10 bar of pressure. Color lines for each fraction of CO<sub>2</sub> in the gas mixture are only guides to the eye.

To make a deep insight in the performance in the different zeolites, **Fig. 2a** collects the CO<sub>2</sub> loadings from the computed adsorption isotherms for the mixture containing 10 % CO<sub>2</sub> in dry air. Among all the zeolites, MFI exhibits the highest uptake for all the pressure range. Loadings of 0.4, 0.7, and 1.2 mol kg<sup>-1</sup> are obtained at 1, 2, and 10 bar of pressure, respectively. Adsorption values are not very high due the relatively low working pressures, but the adsorbed fraction of CO<sub>2</sub> (color graduation) is increased from 0.10 in the bulk mixture to more than 0.7, indicating a very high selective capture towards CO<sub>2</sub>. The AOPs of CO<sub>2</sub> in this structure (**Fig. S8**) show a strong adsorption of CO<sub>2</sub> in the intersections of



the straight channels parallels to the y-axis and the zig-zag channels on the xz-plane. Molecules seem to commensurate well in these adsorption sites, allowing this structure to show the best performance among the studied zeolites, both in terms of uptake and preferential adsorption. From Fig. S8 it can be also observed how zig-zag and parallel channels are progressively filled from the lowest to the highest pressure.

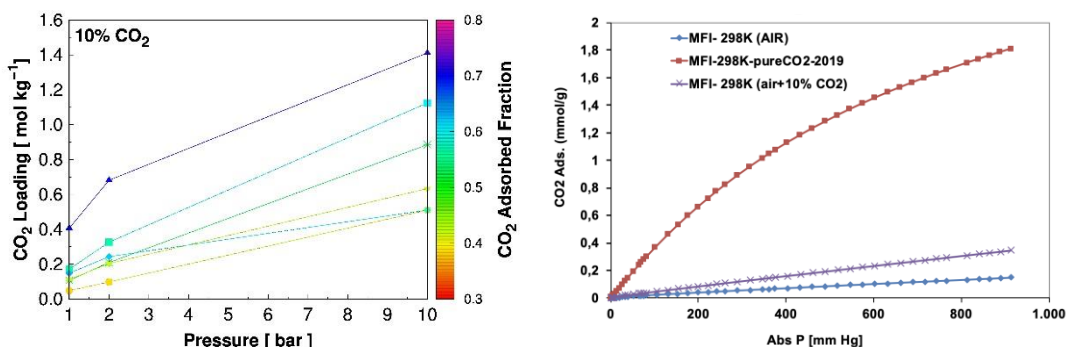


**Figure 2.** (A) Computed CO<sub>2</sub> adsorption loadings in BEA (squares), FAU (circles), FER (circles), ITQ-29 (asterisks), MFI(triangles), and MOR(diamonds) zeolites at room temperature and 1, 2, and 10 bar of pressure for a mixture containing 10 % CO<sub>2</sub> in dry air. The color code shows the CO<sub>2</sub> adsorbed fraction. (B) Experimental adsorption isotherms for MFI zeolite at room temperature for pure CO<sub>2</sub>, synthetic air and a mixture containing 10 % CO<sub>2</sub> in dry synthetic air.

BEA zeolite shows noticeably reduced CO<sub>2</sub> loadings compared to MFI, except at 10 bar in which total pressure it reached *ca.* 1 mol kg<sup>-1</sup>. The slightly widest system of channels explains the lower adsorption. Adsorbed molar fractions of CO<sub>2</sub> are also quite lower, with values between 0.6 and 0.7. The ability of the rest of zeolites to selectively capture CO<sub>2</sub> is even worse or more limited or more restricted, barely increasing adsorbed fractions above 0.5 and showing uptakes of less than 0.3 mol kg<sup>-1</sup> at intermediate pressure. In some structures

(i.e. FAU and ITQ-29), high available pore volume and cage-type topology hinder the fitting of the molecules inside them. On the other hand, the existing preferential adsorption sites in MOR for N<sub>2</sub>, previously described, reduce the CO<sub>2</sub> selective capture, despite having similar pore volume, surface area and channels diameters than BEA.

In order to validate the GCMC predictions, adsorption experiments for the best performing MFI zeolite were carried out. We chose this material for being commercial and, besides, for being the most promising for CO<sub>2</sub> adsorption, and this by a substantial amount (**Figure 2a**). Equilibrium adsorption isotherms for pure CO<sub>2</sub>, synthetic air and a mixture containing 10 % CO<sub>2</sub> in dry synthetic air are shown in **Fig 2b**. The volumetric equipment used does not allow to discriminate the uptake corresponding to carbon dioxide in the mixture, for which the adsorption isotherm of synthetic air was also measured to estimate the contribution of nitrogen and oxygen to the adsorption of the mixture. As seen, the total amount of gas adsorbed for the mixture of 10% CO<sub>2</sub> in air at atmospheric pressure is about 15.3 g/Kg zeolite (0.35 mol/Kg), which is in good agreement with the amount computed for this zeolite at 1 bar. This experimental estimation is also in line with the IAST prediction for a mixture of 10% CO<sub>2</sub> in air evaluated from the experimental adsorption isotherms of air and pure CO<sub>2</sub> (11.4-17.2 g/kg).

### **3.2 CO<sub>2</sub> adsorption capacity of best performing zeolite: PSA estimations**

To compare the performance of each of the studied zeolites in a PSA industrial cycle, we have employed the so-called “Bed Capacity Factor” (BCF) to compare the PSA performance of each structure when using the Skarstrom cycle.<sup>37</sup> This parameter is defined as the adsorption capacity of the column utilized at the end of adsorption step (ADS in **Fig.**

**S3**, incipient breakthrough of the adsorbate) under cyclic steady state operation relative to the maximum capacity of the column under feed gas conditions. For the same operating conditions, the lower this parameter is the better is the PSA performance because the process is able to remove a higher amount of heavy adsorbate from the light product (rich in weak adsorptive). The advantage of BCF parameter compared to others is that it considers simultaneously the effect of the most important variables that determine separation (working capacity, adsorption rate and selectivity). For a single PSA cycle at *isothermal conditions* we obtained the following BCF values: MFI = 0.21; BEA= 0.53; FER = 0.56; MOR = 0.68; ITQ-29 = 0.80; FAU = 0.99. These results are in close agreement with the previously obtained results from GCMC simulations (**Section 3.1**) and confirm that MFI offers quite better performance than the rest of structures for CO<sub>2</sub> capture and separation from the flue gas.

On these grounds, the MFI zeolite is chosen to simulate the PSA dual cycle with three equalization steps at *adiabatic conditions*. Although the PSA model has not been validated for this type of zeolite, it has been validated with experimental results previously.<sup>49,50</sup> See for instance Delgado et al. (<https://doi.org/10.1007/s10450-015-9654-z>) and Brea et al. (<https://doi.org/10.1016/j.cej.2018.08.154>).

As mentioned above, this type of arrangement improves the yield of CO<sub>2</sub> separation in industrial processes. The design specifications of the dual-PSA cycle have been defined as a CO<sub>2</sub> purity in the heavy product above 95% and CO<sub>2</sub> recovery above 90% (calculated as global results for the two coupled cycles). The feed gas velocities of both cycles have been used as input variables to achieve the desired design specifications, resulting in a feed gas velocity of 0.0452 m s<sup>-1</sup> for the rectifying cycle (PSA I) and 0.11 m s<sup>-1</sup> for the stripping cycle (PSA II). A flowsheet with the molar flow rates and stream compositions of the

designed dual cycle is shown in **Fig. S4b**. The performance parameters of each individual cycle and the global ones for the dual cycle are presented in **Table 1**. A CO<sub>2</sub> productivity of **8.24 kg/m<sup>3</sup>/h** is estimated. The energy requirement for evacuation steps has been calculated assuming isentropic compression with efficiency of 60%. From **Fig. S4b**, it is observed that practically dry CO<sub>2</sub> is obtained as final product. This is an advantage (apart from the possibility of treating a humid gas) because further drying of CO<sub>2</sub> is not necessary for using it in other applications.

**Table 1.** Performance parameters of the designed dual-PSA cycle

	PSA I	PSA II	DUAL PSA
CO <sub>2</sub> purity, %	35.400	95.010	<b>95.011</b>
CO <sub>2</sub> recovery, %	91.870	80.070	<b>90.040</b>
CO <sub>2</sub> productivity, kgCO <sub>2</sub> captured/m <sup>3</sup> bed/h	11.400	85.500	<b>8.240</b>
Energy requirement, MJ/kgCO <sub>2</sub> captured	0.589	0.252	<b>0.987</b>

### **3.3 Biomass production and photosynthetic efficiency by microalgae and strain screening**

The first step in the use of microalgae for CO<sub>2</sub> capture is the selection of the right strain. A lot of microalgae and cyanobacteria strains have been investigated at this respect, in most of the cases performing batch cultures, others providing continuous light, and finally using non real flue gases. To obtain reliable figures for further scale-up processes the conditions at which the strains are evaluated must be as close as possible to that prevailing at outdoor. Here, the performance of ten previously reported

microalgae/cyanobacteria has been evaluated. **Fig. 3** shows that the different microalgae have largely different potential. *Scenedesmus* was the most productive, with values up to 1.6 g/L·day, whereas *Nostoc* and *Spirulina* were the less productive, with productivities below 0.5 g/L·day (**Fig. 3A**). *Scenedesmus* strain is widely reported under outdoor production conditions, including in CO<sub>2</sub> capture processes, as it has demonstrated itself to be robust and suitable for outdoor production, even in non-optimal raceway reactors or using wastewaters as the nutrient source<sup>51,52</sup>. In general cyanobacteria show a lower performance than microalgae. These values are the maximal ones because they were obtained in a well-controlled and favorable environment, although under simulated outdoor conditions. The obtained figures compare well with other previously reported. Thus, using *Anabaena* up to 1.0 g/L·day of captured CO<sub>2</sub> was obtained at laboratory scale, it being mainly accumulated at released exopolysaccharides.<sup>53</sup> In terms of photosynthetic efficiency (PE, Eq. (4)) an analogous trend is observed because the light provided was the same for all the experiments and the light utilization is proportional to the biomass productivity (**Fig. 3B**). Crucial information in this figure is the final values, as under optimal laboratory conditions the PE can be as high as 3.0 %, much higher than that typically found in larger plants, i.e. 1%. These figures justify the high potential of microalgae to efficiently use the sunlight to capture CO<sub>2</sub> and to transform it into valuable biomass. In this respect, it has been reported that up to 200 tn/ha·year of CO<sub>2</sub> could be captured by microalgae.<sup>19</sup>

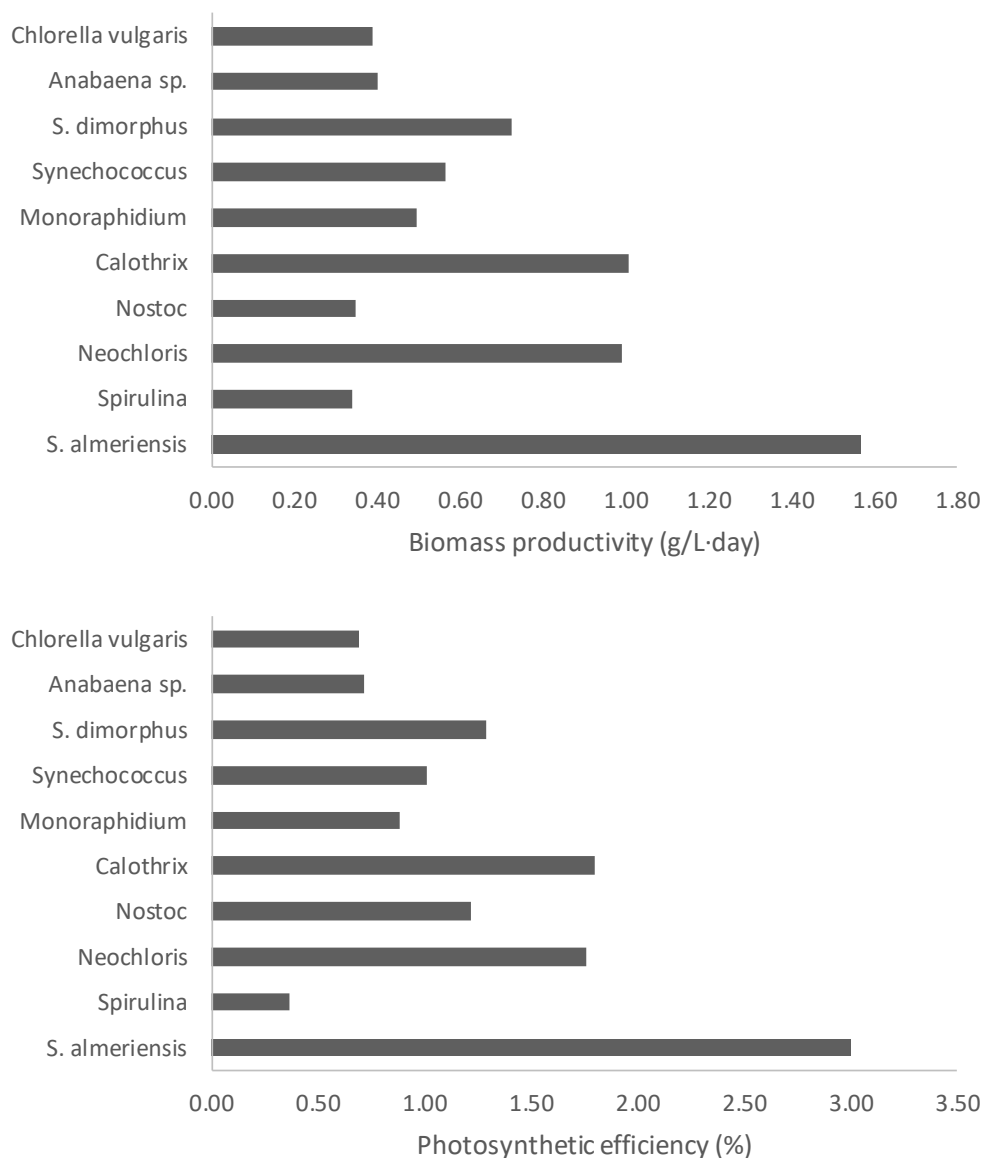


**Figure 3.** Biomass productivity (**top**) and photosynthetic efficiency (**bottom**) of microalgae strains evaluated at laboratory scale.

To analyse the real figures about CO<sub>2</sub> capture and how it is transformed into valuable products the theoretical CO<sub>2</sub> fixation rate and biochemical composition of produced biomass were determined (**Fig. S9** in the **Supporting Information**). Theoretical CO<sub>2</sub>

fixation rate correspond to the amount of CO<sub>2</sub> fixed as biomass on the basis of biomass productivity and total carbon content of the biomass (ranging from 0.40 to 0.51% d.wt., data not shown). In addition to this value, the net CO<sub>2</sub> fixation rate can be larger if the total carbon content of the biomass increases. However, it is not modified too much if the cultures are operated at continuous mode, or if the CO<sub>2</sub> is additionally absorbed into the liquid as dissolved inorganic carbon. At laboratory scale these effects are not relevant. Hence, we consider henceforth the net amount of CO<sub>2</sub> fixed as biomass as a suitable approximate figure of merit. Results confirm that *Scenedesmus* is the most promising strain, showing values up to 2.5 g/L·day, much higher than that obtained when using *Nostoc* or *Spirulina* strains (**Figure S9A**). In terms of biochemical composition carbohydrates and proteins were the most relevant fractions, the lipids content being always lower than 20 %d.wt., except in the case of *Neochloris* that shows a lipids content of 26 %d.wt. (**Figure S9B**). *Neochloris* is a small microalga that accumulates large amounts of lipids, up to 50% under non-growing conditions<sup>54</sup>. This strain has been widely reported as a potential biofuel source as it is even able to grow in wastewaters<sup>55,56</sup>. In the case of *Scenedesmus* the percentage of carbohydrates was really high, up to 53 %d.wt., but it was including higher in the case of *Calothrix* and *Anabaena*, with more than 70 %d.wt. of carbohydrates. In terms of proteins, the strain showing a higher protein content was *Spirulina*, up to 60%d.wt., whereas *Anabaena* and *Calothrix* shows the lowest contents, lower than 20 %d.wt., in spite that all of them are cyanobacteria. Similar biochemical composition to that here showed has been previously described for *Chlorella vulgaris* (<sup>57</sup>), *Scenedesmus* (<sup>58</sup>), and *Neochloris* (<sup>59</sup>). The different biochemical composition of the produced biomass indicates that each one of them could be used for different purposes as biofuels, biofertilizers, animal feed, etc.<sup>60,61</sup> However, the biomass value varies in the

diverse applications so, to achieve a reliable process, it is necessary to identify a target market where the biomass value will be higher than its production cost.<sup>19</sup>

As previously stated, the choosing of the final strain to be used at large scale also depends on the value of the produced biomass and the economic yield of the process (**Fig. S10**). To determine these values a standard value of proteins (1 €/kg), lipids (0.6 €/kg) and carbohydrates (0.3 €/kg) has been considered, these values corresponding to the approximate price of these commodities. All the microalgae/cyanobacteria biomasses produced have an equivalent value, ranging from maximal value of 0.7 €/kg of *Spirulina*, to the minimum value of 0.4 €/kg of *Anabaena* (**Fig. S10A**). It is noticeable the high value of *Neochloris* because this strain have been widely reported as interesting for biodiesel production,<sup>54</sup> in addition to *Nostoc* which has been reported as a robust strain suitable to be produced at large scale.<sup>62</sup> However, *Spirulina* and *Nostoc* were some of the less productive strains. Multiplying the value of the biomass by the biomass productivity, i.e., the economic yield, is a more interesting criterion. The results show that *Scenedesmus* is the most interesting strain in this respect, its economic yield being of 0.87 €/m<sup>3</sup>·day (**Fig. S10B**).

### **3.4 Biomass production and photosynthetic efficiency at outdoor conditions**

Once the optimal strain has been selected, it was tested in real outdoor conditions, using a 100 m<sup>2</sup> pilot scale raceway reactor operated in continuous mode at 0.2 day<sup>-1</sup> during six months from January to June at Almeria (Spain). On this time the solar radiation changes from 11 to 30 MJ/m<sup>2</sup>·day whereas the mean daily temperature ranged from 12°C in winter time to 25°C in summer time. In spite of large variations of solar radiation and



temperature, not only along the days but also in each solar cycle, the cultures of *Scenedesmus* perform adequately, no large contamination problems existing and the culture being stable for long time (**Fig. 4**). Data shows as the biomass productivity increases from 10 to 30 g/m<sup>2</sup>·day from January to June mainly by the increase on solar radiation availability. On this time the photosynthetic efficiency did not change too much, a really high mean value of 2.0% being measured. These values confirm the adequacy of the selected strain to be used in large scale CO<sub>2</sub> capture processes.

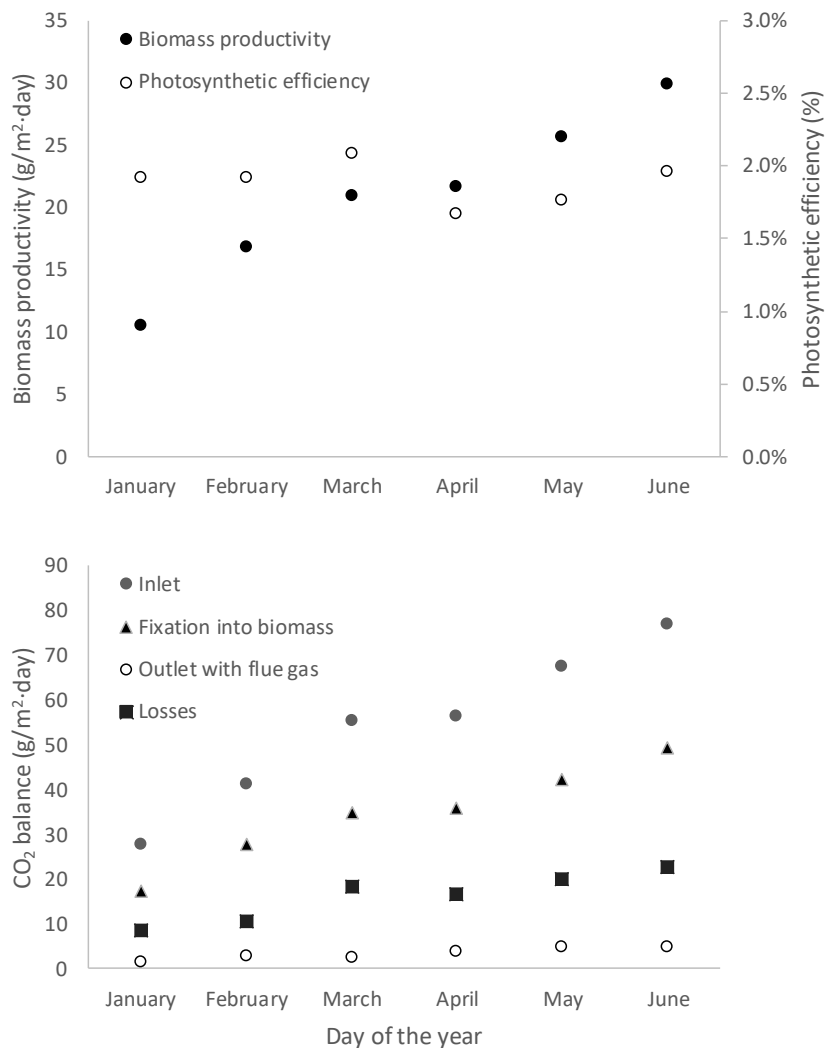


**Figure 4.** Variation of biomass productivity and photosynthetic efficiency (top) and carbon dioxide balance (bottom), in addition to CO<sub>2</sub> inlet and outlet streams, of outdoor continuous cultures of *Scenedesmus almeriensis* in a 100 m<sup>2</sup> pilot scale raceway reactor located in Almeria (Spain).

To determine the real CO<sub>2</sub> capture capacity, the mass flow of CO<sub>2</sub> entering to the reactor was measured, in addition to the net amount of CO<sub>2</sub> fixed into the biomass, and the CO<sub>2</sub> losses with the flue gases exhausting the reactor. The difference between the CO<sub>2</sub> inlet and the CO<sub>2</sub> outlet with the biomass and the flue gases was calculated as overall CO<sub>2</sub>

losses. The results indicate that the CO<sub>2</sub> demand of the system increases when increasing the biomass productivity, due to the control system used to maintain the pH at its optimal value (Fig. 5b). The total CO<sub>2</sub> demand ranged from 27.6 to 76.7 g/m<sup>2</sup>·day. This CO<sub>2</sub> was mainly consumed by the biomass, their values ranging from 17.5 to 49.3 g/m<sup>2</sup>·day. The larger amount of CO<sub>2</sub> supplied with respect to the net amount fixed into the biomass was due to the efficiency of the CO<sub>2</sub> supply system. Thus, CO<sub>2</sub> losses by non-absorption of CO<sub>2</sub> contained into the flue gases injected ranges from 1.4 to 4.8 g/m<sup>2</sup>·day. These values are really minor when comparing with total CO<sub>2</sub> supplied, indicating the adequate performance of the CO<sub>2</sub> gas supply system. However, still a large fraction of CO<sub>2</sub> was lost, ranging from 8.7 to 22.6 g/m<sup>2</sup>·day. These losses can be due to decarbonisation into the entire raceway reactor or carbon outlet with the outlet culture broth when harvesting. Anyway, the total amount of CO<sub>2</sub> demanded by the system was **54 g/m<sup>2</sup>·day**, equivalent to 197 t/ha·year. This means that the CO<sub>2</sub> demand to biomass productivity ratio is 2.58, instead of the 1.83 value theoretically obtained if considering the basic equation of photosynthesis. This is an important fact considering CO<sub>2</sub> emissions at ground level or the increase of inorganic carbon concentration in the exhausted water for its final disposal. On average, the CO<sub>2</sub> fixation into the biomass represent 64.0% of the total CO<sub>2</sub> inlet, whereas CO<sub>2</sub> losses with the exhaust gas represent 9.6% of the total CO<sub>2</sub> inlet, then the remaining CO<sub>2</sub> losses representing up to 26.4% of total CO<sub>2</sub> inlet. Although raceway reactors are the most suitable for CO<sub>2</sub> capture-related processes other technologies has been previously studied. By comparing the performance of *Anabaena* cultures carried out in raceway, tubular photobioreactors and flat panels, the optimal value of 35 g/m<sup>2</sup>·day was achieved in flat panels reactors.<sup>63</sup> However, the scale-up of this technology is still a major issue in microalgae biotechnology field.

#### 4. DISCUSSION

As mentioned in the introduction the purpose of this work is to analyze and compare the capability of CO<sub>2</sub> capture by a physicochemical means (adsorption in porous media) and by biological means (biomass production by microalgae). In this respect, not only the rate of CO<sub>2</sub> capture is of importance, but also the energy requirements of the process and the valorization of the final product.

As regards the former, the separation performance of the proposed dual-PSA process with the best performing zeolite MFI provides a figure of 8 kg m<sup>-3</sup> bed h<sup>-1</sup>, which is substantially higher than previously reported data by microalgae (0.04-0.25 kg m<sup>-3</sup> broth h<sup>-1</sup>)<sup>64</sup> and the data presented in this work: 0.01 kg m<sup>-2</sup> h<sup>-1</sup>. On the other hand the energy requirement is lower than the one of amine scrubbing processes (0.37 kWh/kgCO<sub>2captured</sub> = 1.3 MJ/kgCO<sub>2captured</sub>).<sup>65</sup> As regards the economic aspect, the obtained product (high purity CO<sub>2</sub>) can be used in many applications, such as obtaining carbon monoxide, methane or methanol.

With respect to the biological alternative, it must be born in mind that the CO<sub>2</sub> supply system must be accurately designed to avoid reemission of CO<sub>2</sub> to the atmosphere. Carbon dioxide can be supplied to microalgae cultures by (a) continuous bubbling or (b) on-demand injection. With continuous bubbling of flue gases, the medium becomes acidic and maximum CO<sub>2</sub> use efficiencies of only 8.1 %<sup>66</sup> and 4.2 %<sup>67</sup> have been reported. With on-demand injection of flue gases, a maximum CO<sub>2</sub> use efficiency of 32.8 % in open photobioreactors<sup>68</sup> and 50 % in closed photobioreactors<sup>69</sup> have been determined. In both strategies, the consumption of CO<sub>2</sub> is a function of the design and the operation of the carbonation unit, and finally, of the mass transfer phenomena into the culture. In a different

strategy the CO<sub>2</sub> can be provided dissolved into the culture medium by passing it by a previous carbonation unit, up to 2.0 g/L of total inorganic carbon being dissolved into the culture medium suitable to be consumed by *Anabaena*<sup>70</sup>. Recently the CO<sub>2</sub> capture efficiency in raceway reactors has been re-designed by including a sump into the reactor, and optimizing its design and gas/liquid flow rates. It was demonstrated that under optimal conditions de CO<sub>2</sub> transfer efficiency was up to 98%<sup>71</sup>.

On top of all these considerations, the energy consumption and cost of the biological process must also be analysed. In the case of energy, the major energy inlet on raceway reactors is the power required by the paddlewheel. To minimize the energy consumption, raceway reactors are build following some key rules, as a length to wide ratio of 10, using softer as possible materials, reducing the liquid velocity up to 0.2 m/s, and minimizing the presence of bends and other structural parts that disturb the flow along the channels<sup>72</sup>. Recently the design of this type of reactors has been reviewed to minimize its energy consumption. In this respect a new Low Energy Algae Reactor (LEAR Patent EP2875724A1) has been patented. Thus, energy consumption in raceway reactors can be reduced from 20 to 1 W/m<sup>3</sup>,<sup>21</sup> or including below 1 W/m<sup>3</sup> if using LEAR system. During the operation of the 100 m<sup>2</sup> pilot scale raceway reactor the measured energy consumption was 2 W/m<sup>3</sup>, thus it being equivalent to 0.48 MJ/kg of CO<sub>2</sub> captured, which is substantially lower than the chemical (amines scrubbing) and physicochemical (zeolite adsorption) procedures.

In **Fig. 5** the influence of biomass productivity and specific energy consumption on the raceway reactor into the specific energy consumption per kg of CO<sub>2</sub> captured is analysed. It is confirmed that microalgae-based processes have lower energy consumption

that amines-based processes only when specific energy consumption of the reactor are lower than  $20 \text{ W/m}^3$  and at biomass productivities are higher than  $25 \text{ g/m}^2\cdot\text{day}$ . When comparing with zeolites-based processes the microalgae have lower energy consumption only when operating at specific energy consumption in the raceway reactor lower than  $2 \text{ W/m}^3$  and biomass productivities higher than  $15 \text{ g/m}^2\cdot\text{day}$ . Anyway, these figures show that the microalgae-based processes for  $\text{CO}_2$  capture are in the same range of energy consumption than low energy demanding technologies as PSA with zeolites. In terms of cost, the biomass production cost in this type of raceway reactors can be reduced till  $2.1 \text{ €/kg}$  when using flue gases and minimum manpower ( $0.1 \text{ men/ha}$ ), it being equivalent to a  $\text{CO}_2$  capture cost of  $0.8 \text{ €/kg}$ <sup>73</sup>. This production cost is much higher than conventional price of industrial pure  $\text{CO}_2$ , ranging from  $0.1\text{-}0.2 \text{ €/kg}$ . However, the price of microalgae biomass is much higher than of pure  $\text{CO}_2$ , minimum values of  $5 \text{ €/kg}$  being reported<sup>74</sup>. Considering this price for the biomass, the value of  $\text{CO}_2$  contained into the biomass is  $1.9 \text{ €/kg}$ , much higher than estimated  $\text{CO}_2$  capture cost of  $0.8 \text{ €/kg}$ . Thus, to achieve a suitable commercial process for  $\text{CO}_2$  capture, it is necessary to produce valuable biomass otherwise the production cost will be higher than the  $\text{CO}_2$  emission taxes<sup>19</sup>.

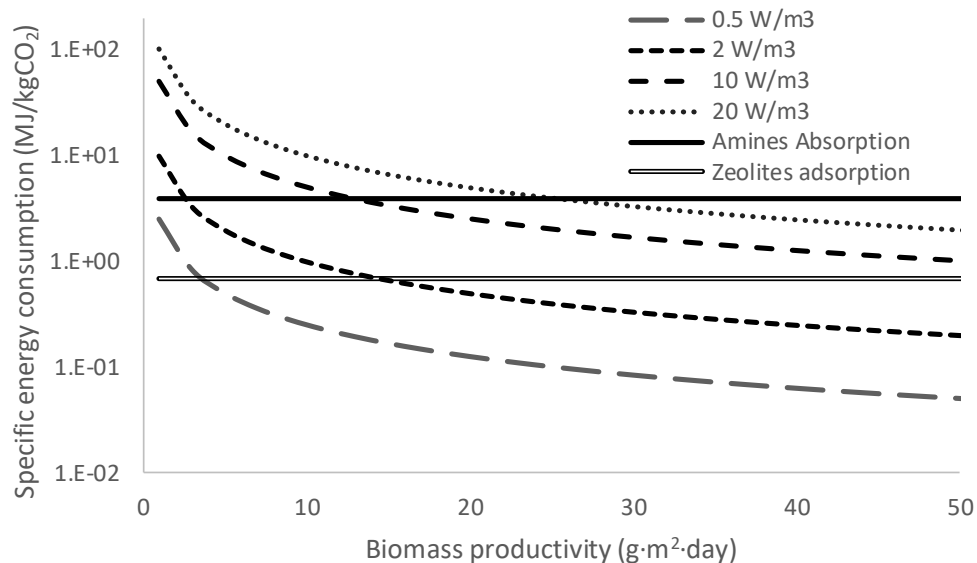


**Figure 5.** Variation of energy consumption of microalgae-based processes as a function of biomass productivity and specific energy consumption of the reactor.

## 5. CONCLUSIONS

The alternative capabilities of a physicochemical (adsorption in porous media) and a biological process (biomass production by microalgae) to capture CO<sub>2</sub> from flue gases has been analysed, assessed and compared.

In connection to the physicochemical alternative, GEMC simulations and adsorption experiments demonstrate that commercial zeolite MFI is the best candidate to capture this gas due to the morphology and crystalline structure of this material. Numerical simulation of a dual PSA cycle suitable for industrial implementation confirms this finding and provides an estimated value for CO<sub>2</sub> capture of 8 kg m<sup>-3</sup> bed h<sup>-1</sup> and an energy consumption of 0.987 MJ/Kg of captured CO<sub>2</sub>.

In connection to the biological alternative, it is demonstrated that microalgae-based processes for capturing CO<sub>2</sub> from flue gases can be performed, being reliable at real outdoor operation conditions for more than six months. The key factors determining the reliability of the process are the selection of adequate strains and technologies. From the up to ten microalgae/cyanobacteria strains evaluated, the fast growing and robust *Scenedesmus almeriensis* was the more productive, up to 0.06 kg m<sup>-3</sup> broth h<sup>-1</sup>. The production of this strain in a 100 m<sup>2</sup> pilot scale raceway reactor at real outdoor conditions was demonstrated, allowing to capture up to 54 gCO<sub>2</sub>/m<sup>2</sup>·day in average from January to June. The strategy of on-demand supply of CO<sub>2</sub> and optimal mass transfer capacity into the reactor allows to capture up to 2.58 kgCO<sub>2</sub> per kg of produced biomass, only 9.6% of the supplied CO<sub>2</sub> being lost to the atmosphere. Energy consumption of the process was estimated at 0.48 MJ/kgCO<sub>2</sub>, the unitary cost being 0.8 €/kg of CO<sub>2</sub>. The energy consumption is lower than the physicochemical process, but the cost is much high than regular price of pure CO<sub>2</sub>. However, value of the microalgae biomass is much higher thus it being concluded that captured CO<sub>2</sub> have a value equivalent to 1.9 €/kg. These figures provide a realistic scenario about the potential application of microalgae to CO<sub>2</sub> capture related processes.

Although the major bottleneck of microalgae-based processes is the necessity of high sunlight and land availability, this technology can be an alternative for diffuse CO<sub>2</sub> emission from small industries and farms, among others. Physicochemical processes do not depend on ambient conditions and land availability but rely on a suitable use and management of the resulting stream of pure CO<sub>2</sub> obtained.



## ACKNOWLEDGEMENTS

This study was carried out with the financial support of Junta de Andalucía, grant FQM 1851 and the company, SETEC. We are grateful for the practical assistance kindly given by the staff of the Las Palmerillas Experimental Station, part of the Cajamar Foundation.

## 6. REFERENCES

- 1 Anonymous, Paris Agreement, [https://ec.europa.eu/clima/policies/international/negotiations/paris\\_en](https://ec.europa.eu/clima/policies/international/negotiations/paris_en), (accessed 16 March 2019).
- 2 M. Collins, R. Knutti, J. Arblaster, J.-L. Dufresne, T. Fichefet, P. Friedlingstein, X. Gao, W. J. Gutowski, T. Johns, G. Krinner, M. Shongwe, C. Tebaldi, A. J. Weaver and M. Wehner, *Clim. Change 2013 Phys. Sci. Basis Contrib. Work. Group Fifth Assess. Rep. Intergov. Panel Clim. Change*, 2013, 1029–1136.
- 3 E. Herzog, H., Drake E., Adams, *EM Featrure*, 1997, 22–24.
- 4 O. US EPA, Sources of Greenhouse Gas Emissions, <https://www.epa.gov/ghgemissions/sources-greenhouse-gas-emissions>, (accessed 16 March 2019).

2019).

- 5 C.-H. Yu, C.-H. Huang and C.-S. Tan, *Aerosol Air Qual. Res.*, 2012, **12**, 745–769.
- 6 G. T. Rochelle, *Science*, 2009, **325**, 1652–1654.
- 7 J.-L. Li and B.-H. Chen, *Sep. Purif. Technol.*, 2005, **41**, 109–122.
- 8 M. J. Tuinier, H. P. Hamers and M. van Sint Annaland, *Int. J. Greenh. Gas Control*, 2011, **5**, 1559–1565.
- 9 Global CCS Institute, *The global status of ccs: 2011*, 2011.
- 10 M. T. Ho, G. W. Allinson and D. E. Wiley, *Ind. Eng. Chem. Res.*, 2008, **47**, 4883–4890.
- 11 Q. Wang, J. Luo, Z. Zhong and A. Borgna, *Energy Environ. Sci.*, 2010, **4**, 42–55.
- 12 Z. Zhao, Z. Li and Y. S. Lin, *Ind. Eng. Chem. Res.*, 2009, **48**, 10015–10020.
- 13 J. M. Vicent-Luna, J. J. Gutiérrez-Sevillano, J. A. Anta and S. Calero, *J. Phys. Chem. C*, 2013, **117**, 20762–20768.
- 14 E. Hughes and J. R. Benemann, *Energy Convers. Manag.*, 1997, **38**, S467–S473.
- 15 U. B. Singh and A. S. Ahluwalia, *Mitig. Adapt. Strateg. Glob. Change*, 2013, **18**, 73–95.
- 16 S.-H. Ho, C.-Y. Chen, D.-J. Lee and J.-S. Chang, *Biotechnol. Adv.*, 2011, **29**, 189–198.
- 17 J. C. M. Pires, M. C. Alvim-Ferraz, F. G. Martins and M. Simões, *Renew. Sustain. Energy Rev.*, 2012, **16**, 3043–3053.
- 18 W. Zhou, J. Wang, P. Chen, C. Ji, Q. Kang, B. Lu, K. Li, J. Liu and R. Ruan, *Renew. Sustain. Energy Rev.*, 2017, **76**, 1163–1175.
- 19 F. G. Acien, C. V. González-López, J. M. Fernández-Sevilla and E. Molina-Grima, *Appl. Microbiol. Biotechnol.*, 2012, **96**, 577–586.

- 20 M. R. Tredici, *Biofuels*, 2010, **1**, 143–162.
- 21 J. L. Mendoza, M. R. Granados, I. de Godos, F. G. Acién, E. Molina, C. Banks and S. Heaven, *Biomass Bioenergy*, 2013, **54**, 267–275.
- 22 J. L. Mendoza, M. R. Granados, I. de Godos, F. G. Acién, E. Molina, S. Heaven and C. J. Banks, *Bioresour. Technol.*, 2013, **137**, 188–195.
- 23 R. K. Desai, M. Streefland, R. H. Wijffels and M. H. M. Eppink, *Green Chem.*, , DOI:10.1039/c3gc42631a.
- 24 S. De Caralt, M. J. Uriz and R. H. Wijffels, *J. Mar. Biol. Assoc. U. K.*, , DOI:10.1017/S0025315407056846.
- 25 F. G. Acién, C. Gómez-Serrano, M. M. . Morales-Amaral, J. M. Fernández-Sevilla and E. Molina-Grima, *Appl. Microbiol. Biotechnol.*, 2016, **100**, 9013–9022.
- 26 S. Venkata Mohan, M. V. Rohit, P. Chiranjeevi, R. Chandra and B. Navaneeth, *Bioresour. Technol.*, , DOI:10.1016/j.biortech.2014.10.056.
- 27 D. Dubbeldam, S. Calero, D. E. Ellis and R. Q. Snurr, *Mol. Simul.*, 2015, **42**, 81–101.
- 28 D. Dubbeldam, A. Torres-Knoop and K. S. Walton, *Mol. Simul.*, 2013, **39**, 1253–1292.
- 29 A. Garcia-Sanchez, C. O. Ania, J. B. Parra, D. Dubbeldam, T. J. H. Vlugt, R. Krishna and S. Calero, *J. Phys. Chem. C*, 2009, **113**, 8814–8820.
- 30 A. Martin-Calvo, E. Garcia-Perez, A. Garcia-Sanchez, R. Bueno-Perez, S. Hamad and S. Calero, *Phys. Chem. Chem. Phys.*, 2011, **13**, 11165–11174.
- 31 S. W. Rick, *J. Chem. Phys.*, 2004, **120**, 6085–6093.
- 32 T. J. H. Vlugt and M. Schenk, *J. Phys. Chem. B*, 2002, **106**, 12757–12763.
- 33 S. Calero, D. Dubbeldam, R. Krishna, B. Smit, T. J. H. Vlugt, J. F. M. Denayer, J. A. Martens and T. L. M. Maesen, *J. Am. Chem. Soc.*, 2004, **126**, 11377–11386.

- 34 R. Krishna and J. M. van Baten, *Langmuir*, 2010, **26**, 2975–2978.
- 35 S. Effendy, C. Xu and S. Farooq, *Ind. Eng. Chem. Res.*, 2017, **56**, 5417–5431.
- 36 J. Park, R. P. Lively and D. S. Sholl, *J Mater Chem A*, 2017, **5**, 12258–12265.
- 37 R. R. Vemula and S. Sircar, *AIChE J.*, **63**, 4066–4078.
- 38 A. L. Myers and J. M. Prausnitz, *AIChE J.*, 1965, **11**, 121–127.
- 39 I. Langmuir, *J. Am. Chem. Soc.*, 1918, **40**, 1361–1403.
- 40 C. A. Grande and R. Blom, *Energy Procedia*, 2012, **26**, 2–14.
- 41 M. Barceló-Villalobos, J. L. Guzmán Sánchez, I. Martín Cara, J. A. Sánchez Molina and F. G. Acién Fernández, *Algal Res.*, 2018, **35**, 91–97.
- 42 J. M. Fernández-Sevilla, E. Molina-Grima, F. García-Camacho, F. G. Acién and J. A. Sánchez-Pérez, *Appl. Microbiol. Biotechnol.*, 1998, **50**, 199–205.
- 43 E. Molina Grima, F. García Camacho, J. A. Sánchez Pérez, F. G. Acién, J. M. M. Fernández Sevilla, J. A. Sánchez Pérez, F. G. Acién Fernández and J. M. M. Fernández Sevilla, *J. Appl. Phycol.*, 1996, **8**, 529–534.
- 44 G. Kochert, *Handb. Phycol. Methods*, 1978, **2**, 95–97.
- 45 C. V. González López, M. del C. Cerón García, F. G. Acién Fernández, C. Segovia Bustos, Y. Chisti and J. M. Fernández Sevilla, *Bioresour. Technol.*, 2010, **101**, 7587–7591.
- 46 S. Sircar, *Ind. Eng. Chem. Res.*, 2006, **45**, 5435–5448.
- 47 J.-R. Li, R. J. Kuppler and H.-C. Zhou, *Chem. Soc. Rev.*, 2009, **38**, 1477–1504.
- 48 I. Matito-Martos, A. Martín-Calvo, J. J. Gutiérrez-Sevillano, M. Haranczyk, M. Doblare, J. B. Parra, C. O. Ania and S. Calero, *Phys Chem Chem Phys*, 2014, **16**, 19884–19893.
- 49 J. A. Delgado, V. I. Agueda, M. A. Uguina, J. L. Sotelo and P. Brea, *Adsorption*, 2015, **21**, 107–123.

- 50 P. Brea, J. A. Delgado, V. I. Águeda and M. A. Uguina, *Chem. Eng. J.*, 2019, **355**, 279–289.
- 51 M. M. Morales-Amaral, C. Gómez-Serrano, F. G. Acién, J. M. Fernández-Sevilla and E. Molina-Grima, *Algal Res.*, 2015, **9**, 297–305.
- 52 T. Duarte-Santos, J. L. Mendoza-Martín, F. G. Acién Fernández, E. Molina, J. A. Vieira-Costa and S. Heaven, *Bioresour. Technol.*, 2016, **212**, 72–81.
- 53 J. F. S. Fernández, C. V. González-López, F. G. A. Fernández, J. M. F. Sevilla and E. M. Grima, *Appl. Microbiol. Biotechnol.*, , DOI:10.1007/s00253-011-3683-7.
- 54 J. Pruvost, G. Van Vooren, G. Cogne and J. Legrand, *Bioresour. Technol.*, 2009, **100**, 5988–5995.
- 55 L. Gouveia, A. E. Marques, T. L. Da Silva and A. Reis, *J. Ind. Microbiol. Biotechnol.*, 2009, **36**, 821–826.
- 56 C. Gómez-Serrano, M. M. Morales-Amaral, F. G. Acién, R. Escudero, J. M. Fernández-Sevilla and E. Molina-Grima, *Appl. Microbiol. Biotechnol.*, 2015, **99**, 6931–6944.
- 57 C. D. Calixto, J. K. da Silva Santana, E. B. de Lira, P. G. P. Sassi, R. Rosenhaim, C. F. da Costa Sassi, M. M. da Conceição and R. Sassi, *Bioresour. Technol.*, 2016, **221**, 438–446.
- 58 L. Yao, J. A. Gerde, S. L. Lee, T. Wang and K. A. Harrata, *J. Agric. Food Chem.*, 2015, **63**, 1773–1787.
- 59 C. A. Popovich, C. Damiani, D. Constenla, A. María Martínez, H. Freije, M. Giovanardi, S. Pancaldi and P. I. Leonardi, , DOI:10.1016/j.biortech.2012.02.121.
- 60 Q. Hu, M. Sommerfeld, E. Jarvis, M. Ghirardi, M. Posewitz, M. Seibert and A. Darzins, 2008, **54**, 621–639.
- 61 A.-M. Lakaniemi, O. H. Tuovinen and J. A. Puhakka, *Bioresour. Technol.*, 2013, **135**, 222–31.

- 62 R. Piccardi, A. Frosini, M. R. Tredici and M. C. Margheri, *J. Appl. Phycol.*, 2000, **12**, 543–547.
- 63 M. E. Clares, J. Moreno, M. G. Guerrero and M. García-González, *J. Biotechnol.*, 2014, **187**, 51–55.
- 64 A. Ghorbani, H. R. Rahimpour, Y. Ghasemi, S. Zoughi and M. R. Rahimpour, *Renew. Sustain. Energy Rev.*, 2014, **35**, 73–100.
- 65 G. T. Rochelle, *Science*, 2009, **325**, 1652–1654.
- 66 Z. Cheng-wu, O. Zmora, R. Kopel and A. Richmond, *Aquaculture*, 2001, **195**, 35–49.
- 67 Q. Hu, N. Kurano, M. Kawachi, I. Iwasaki and S. Miyachi, *Appl. Microbiol. Biotechnol.*, 1998, **49**, 655–662.
- 68 J. Doucha, F. Straka, K. Lívanský and K. Lívanský, *J. Appl. Phycol.*, 2005, **17**, 403–412.
- 69 F. Camacho Rubio, F. G. Acién Fernández, J. A. Sánchez Pérez, F. García Camacho and E. Molina Grima, *Biotechnol. Bioeng.*, 1999, **62**, 71–86.
- 70 C. V. V González-López, F. G. A. Fernández, J. M. M. Fernández-Sevilla, J. F. S. Fernández, E. M. Grima, C. V. González-López, F. G. Acién Fernández, J. M. Fernández-Sevilla, J. F. Sánchez Fernández, E. Molina Grima, C. V. V González-López, F. G. Acién Fernández, J. M. M. Fernández-Sevilla, J. F. Sánchez Fernández, E. Molina Grima, F. G. A. Fernández, J. M. M. Fernández-Sevilla, J. F. S. Fernández and E. M. Grima, *Biotechnol. Bioeng.*, 2012, **109**, 1637–1650.
- 71 I. de Godos, J. L. Mendoza, F. G. Acién, E. Molina, C. J. Banks, S. Heaven and F. Rogalla, *Bioresour. Technol.*, 2014, **153**, 307–314.
- 72 J. C. Weissman and R. P. Goebel, *Design and analysis of microalgal open pond systems for the purpose of producing fuels: A subcontract report*, 1987.
- 73 F. G. Acién, J. M. Fernández, J. J. Magán and E. Molina, *Biotechnol. Adv.*, 2012,

**30**, 1344–1353.

74 P. Spolaore, C. Joannis-Cassan, E. Duran and A. Isambert, *J. Biosci. Bioeng.*, 2006, **101**, 87–96.

